scientific reports

Check for updates

OPEN

Plasma-assisted MnO surface engineered activated carbon felt for enhanced heavy metal adsorption

Chandrika Ashwinikumar Pal[1], Yu-Lim Choi[1], Lakshmi Prasanna Lingamdinne[1], Rakesh Kulkarni[1], Rama Rao Karri[2]✉, Janardhan Reddy Koduru[1]✉ & Yoon-Young Chang[1]✉

This study explores the enhanced adsorption performance of activated carbon felt (ACF) for Cu(II) and Cd(II) ions, achieved using a dual-synergistic approach combining MnO coating and plasma treatment. ACF's intrinsic properties, including a high surface area (~1000–2000 m²/g), large porosity, and excellent mechanical stability, make it a promising material for environmental applications. However, its limited surface functional groups hinder its adsorption efficiency for heavy metals. Conventional acid treatments, though effective in introducing functional groups, compromise ACF's structural integrity and pose environmental hazards. The non-thermal plasma method addresses these challenges by introducing oxygen-rich functional groups and MnO species without using harmful chemicals, preserving the material's mechanical and morphological properties. This study addresses key challenges in adsorption technologies, such as inefficiencies in multi-contaminant systems and adsorbent degradation through plasma-aided modifications. The synergistic modification enhances adsorption performance by leveraging mechanisms such as ion exchange, complexation, and co-precipitation. Adsorption experiments revealed maximum adsorption capacities of 163.39 mg/g for Cu(II) and 214.59 mg/g for Cd(II), with an extended equilibrium time of 720 min at pH 5. This research highlights the significance of plasma-aided modification strategies for developing sustainable and efficient heavy metal adsorbents, contributing to advancements in wastewater treatment technologies.

Keywords Adsorbent material, Plasma surface engineering, Activated carbon felt, Environmental remediation, Water treatment

Heavy metals, such as copper (Cu(II)) and cadmium (Cd(II)), pose significant environmental and health risks due to their persistence and toxicity, even at trace concentrations. Cu(II) is known to cause gastrointestinal and liver damage, while Cd(II) is a potent carcinogen associated with kidney and bone damage[1]. The World Health Organization (WHO) has set strict guidelines for their concentration in water, recommending a maximum of 5.0 µg/L for Cd(II) in natural waters and 3.0 mg/L for Cu(II) in inland waters, with a more stringent limit of 0.05 mg/L for drinking water. Consequently, effective removal of these contaminants from wastewater is essential for protecting aquatic ecosystems and public health[2].

Several treatment methods have been developed to mitigate contamination from mining runoff, industrial discharges, and agricultural runoff, including adsorption, chemical precipitation, ion exchange, and membrane filtration. Among these, adsorption is the most widely used due to its simplicity, cost-effectiveness, and high efficiency. Unlike chemical precipitation, which generates large waste volumes, or ion exchange, which is expensive, adsorption offers a more sustainable and scalable solution[3]. The process relies on surface interactions between adsorbents and contaminants, where adsorbents such as activated carbon[4,5], carbon felts[6], zeolites[7], and biochar[8] are commonly employed. However, powdered adsorbents often face challenges like inefficient regeneration and difficult recovery[9].

Recent advancements in adsorption technology have introduced Activated Carbon Felts (ACF), which have proven particularly effective in removing Cu(II) and Cd(II) from wastewater[6,10,11]. ACFs offer several

[1]Department of Environmental Engineering, Kwangwoon University, Seoul 01897, Republic of Korea. [2]Petroleum and Chemical Engineering, Faculty of Engineering, Universiti Teknologi Brunei, Bandar Seri Begawan BE1410, Brunei Darussalam. ✉email: kramarao.iitd@gmail.com; reddyjchem@gmail.com; yychang@kw.ac.kr

advantages, including a high surface area, excellent porosity, and the ability to modify surface properties to enhance adsorption capacity. Surface modification techniques, both chemical and physical, have been employed to improve the efficiency of ACFs. These modifications introduce functional groups that facilitate stronger interactions with heavy metal ions, thereby increasing adsorption efficiency. Despite their potential for large-scale applications, ACFs require further optimisation to address challenges related to regeneration and long-term stability[6,12].

Surface modification techniques for ACFs can be broadly categorised into mechanical, chemical, and physical methods. Mechanical methods enhance surface area but may compromise the structural integrity of the material. Chemical modifications, such as treatment with nitric acid (HNO_3) or sulfuric acid (H_2SO_4), introduce functional groups that improve adsorption but can degrade the ACF structure. Physical treatments, such as non-thermal plasma treatment, modify surface properties without affecting the bulk material[13,14]. Plasma treatment offers a dry, reagent-free alternative that enhances adsorption but has shown limited effectiveness in isolation. Combining plasma treatment with chemical activation has been shown to improve adsorption capacity, though further optimisation of parameters such as power, gap distance, and treatment duration is needed[10,15].

In this study, we addressed the existing research gap by investigating the deeper mechanisms of surface modification of ACFs through the combined use of $KMnO_4$ coating and plasma treatment. Our approach not only enhances the removal efficiency of Cu(II) and Cd(II) ions from water but also provides insights into the long-term stability and regeneration of adsorptive sites. However, the presence of phosphates and divalent cationic species reduced their adsorptive effectiveness. Recycling tests confirmed that the modified ACFs remained effective for up to five cycles, with a removal efficiency of at least 60%. Utilising a fixed bed column for adsorption testing and employing micro and spectroscopic methods, we assessed the performance of the modified ACFs in heavy metal removal. The novel integration of plasma treatment allowed for a detailed examination of chemical changes within the ACFs, revealing the synergistic effects with $KMnO_4$ that significantly improved performance. The findings highlight the potential of surface-modified ACFs for sustainable industrial wastewater treatment and robust environmental remediation, although further optimisation is necessary to improve performance under varying conditions.

Experimental section

Materials

Activated carbon felt made from polyacrylonitrile (ACF) was bought from Korea Activated Carbon Felt Ltd. (South Korea); potassium permanganate ($KMnO_4$), sodium hydroxide (NaOH) (solid pellets) and hydrochloric acid (HCl) were acquired from Samchun Pure Chemical Co. Ltd. (Korea). Cadmium nitrate and copper nitrate were purchased from Junsei Chemicals (Korea). All the procured reagents were of analytical grades and were commissioned without any further procedures.

Experimental procedure for fabrication of modified ACF

Preparation of MnO-PT-ACF [modified ACF

The ACF material was first washed with a 1:1 mixture of hot water and ethanol to remove surface impurities, then dried at 65 °C for 24 h and cut to 120 mm x 20 mm dimensions. It was pre-treated with $KMnO_4$, oxidation by soaking and stirring for 1 h at room temperature. Next, the $KMnO_4$, /ACF was subjected to plasma treatment by placing it in a 3 mm gap of the DBD reactor, with O_2 (20 mL/min) and Ar (5 L/min) gas flows and varying reactor parameters as shown in Fig. 1. Initially, various plasma treatment parameters were tested with a 0.1 M $KMnO_4$ concentration, adjusting power between 50 W and 200 W and exposure times from 20 s to 10 min to optimise the adsorption of Cu(II) and Cd(II). After determining the optimal plasma treatment conditions for the $KMnO_4$ concentration, further studies were conducted using concentrations ranging from 0.01 to 1.0 M. In this study, the unmodified adsorbent is referred to as Untreated ACF (Raw), the adsorbent treated with $KMnO_4$ and dried is called MnO (MnO-ACF), the plasma-treated ACF is designated as PT-ACF, and the adsorbent pre-treated with $KMnO_4$, and plasma is labelled as MnO-PT-ACF, collectively referred to as modified ACF in the manuscript.

Plasma equipment details

The experimental device for atmospheric plasma surface modification of ACF, which is a non-thermal RF-plasma power supply equipped with the power of 220VAC, Single phase 50 ~ 60 Hz; RF frequency 13.56 MHz (Atmospheric process plasma, South Korea). Model name: Q-MyPL Auto 150–220,225 A is selected as the reactor in the dielectric barrier discharge device. Its effective radius (containing material part) is 150 mm, and the discharge gap is 3 mm.

Batch adsorption studies

The evaluation of Cu(II) and Cd(II) adsorption capacity on the modified adsorbents was conducted using batch adsorption tests. Solutions were prepared by diluting stock solutions (1000 mg/L) of Cu(II) and Cd(II) to a concentration of 20 mg/L in 50 mL polyethylene Falcon tubes. A fixed adsorbent dosage of 0.5 g/L was used, and pH was adjusted between 2 and 8 using 0.1 M HCl and 0.1 M NaOH. After a reaction time of 720 min, samples were filtered through 0.45 µm discs and analysed for Cu(II) and Cd(II) concentrations using inductively coupled plasma-optical emission spectroscopy. For the kinetic study, samples were taken at intervals (5–1440 min) from a 250 mL initial solution of 20 mg/L Cu(II) and Cd(II). The adsorption capacity, Qt (mg/g), was calculated using the appropriate equation based on the synthesised adsorbent at time "t" and the concentration of the metal ions as shown in Eq. (1).

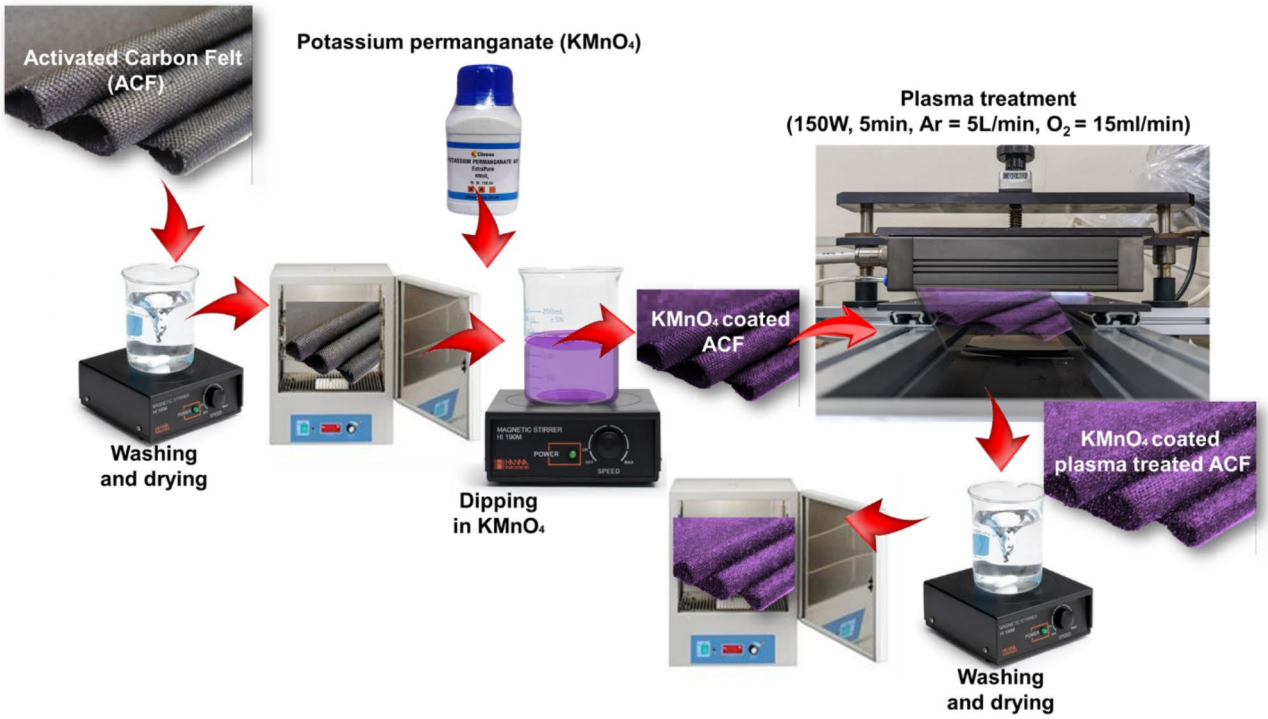

Fig. 1. Schematic representation of the experimental process for pre-treated MnO-coated plasma surface modification of activated carbon felt (modified ACF).

$$Q_t = \left(\frac{C_0 - C_t}{m}\right) \mathrm{V} \tag{1}$$

Herein, Ct is the concentration of Cu(II) and Cd(II) adsorbate in mg/L at time t; V is the volume of the reaction (L), and m is the mass (g) of the adsorbent. In the thermodynamic experiments, a thermostatic water bath maintained precise temperature control at 298 K, 308 K, and 318 K with a constant pH of 5. Isothermal studies were conducted with initial concentrations ranging from 10 to 200 mg/L. All experiments were conducted in duplicate sets, and the average values were considered and reported.

Impact of co-existing ions and regeneration studies

The potential of modified Activated Carbon Felt (ACF) was evaluated for the adsorptive removal of Cu(II) and Cd(II) ions. The study used a 0.5 g/L dosage of modified ACF in a 50 mL solution of 20 mg/L concentration of the metals. The adsorption efficiency was tested at pH 5, with varying metal ion concentrations of 1, 25, 50, and 100 mg/L. These ions included potassium (K^+), nitrates (NO_3^-), sodium (Na^+), sulfates (SO_4^{2-}), calcium (Ca^{+2}), chlorides (Cl^-), magnesium (Mg^{+2}), and phosphates (PO_4^{3-}). The adsorption-desorption conditions were optimised, focusing on nitric acid regeneration through a sonication-assisted pickling process. In this method, 0.5 g/L of modified ACF was immersed in a 250 mL metal solution for 720 min at 298 K to reach equilibrium. Following this, the adsorbent was regenerated using sonication for 5 to 60 min, with nitric acid concentrations ranging from 1 to 15%. The optimal conditions for the regeneration process were established, and over five cycles of adsorption-desorption were applied to assess recyclability. The parameters were chosen based on relevant literature, experimental feasibility, and the aim to maximise treatment effectiveness while ensuring practical, real-world relevance.

Column studies

For continuous column flow studies, a 5.5 cm column with a 3 cm bed height was packed with plasma-modified ACF in a quartz tube. A flow rate of 0.5 mL/min was maintained, and Cu(II) and Cd(II) solutions were set at 5.0 mg/L concentrations. Aliquots were collected daily until the metal ion concentration reached exhaustion. The residual metal concentrations in the effluent were measured using ICP-OES.

Results and discussions

Optimisation of plasma surface modification parameters

Experiments with different plasma power (watts) and exposure times to determine the optimum plasma parameters and validate the optimal $KMnO_4$ concentration for Cu(II) and Cd(II) adsorption on modified ACF. It is apparent from the results, which are presented in Fig. 2a,b, that the maximum adsorption of the heavy metals was accomplished with a plasma power of 150 W and a 5-minute exposure duration for the adsorption of Cu(II) and Cd(II). Increasing the plasma power over longer exposure durations may provide larger discharge

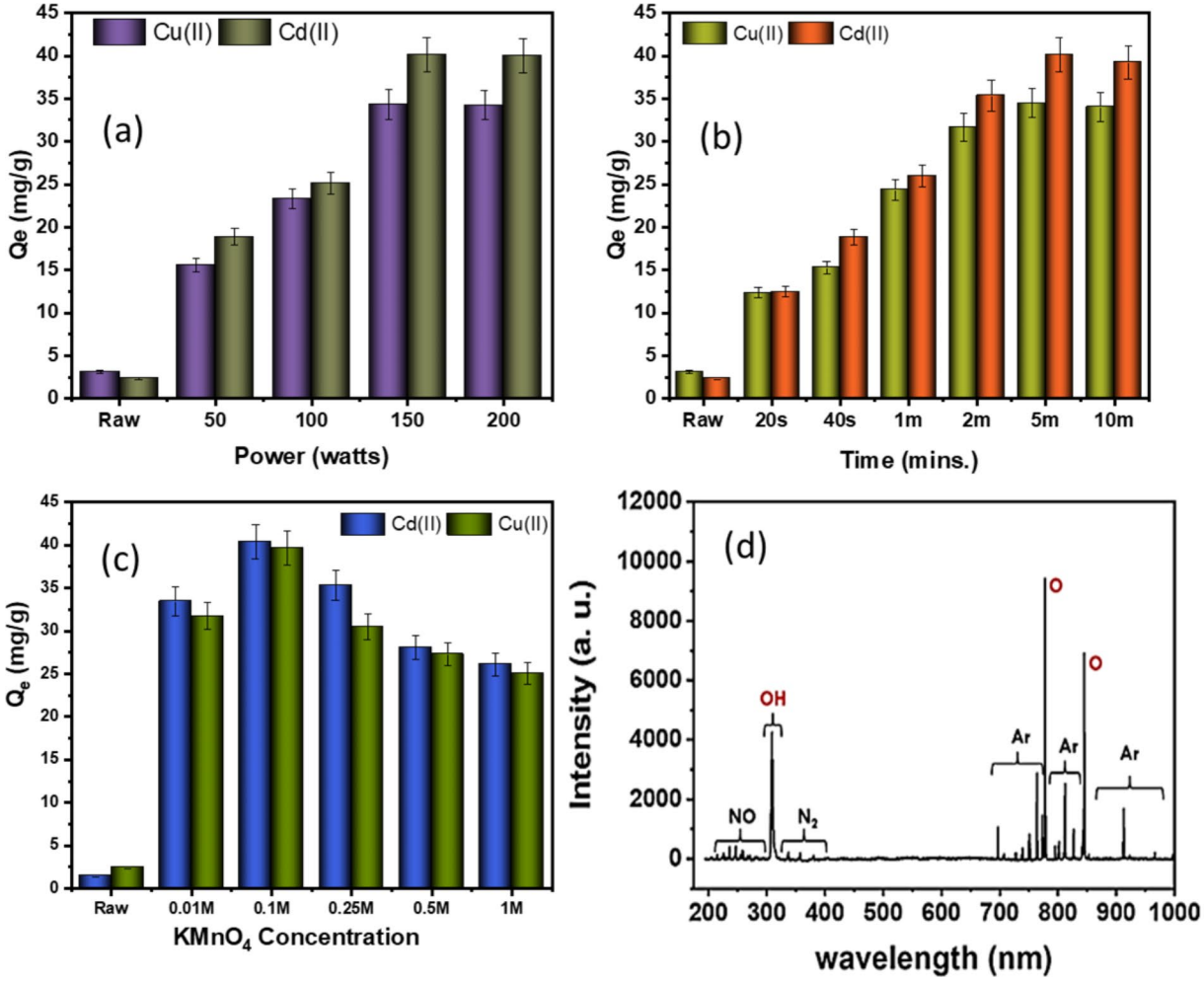

Fig. 2. Adsorption capacities of Cu(II) and Cd(II) on modified ACF with (**a**) plasma power variation, (**b**) plasma exposure time, (**c**) concentration of $KMnO_4$, and (**d**) OES spectra of active plasma species.

effects of plasma species, which could also cause the ACF's overall porosity structure to be over-etched and collapsed[16]. These findings agree with prior studies on ACF plasma treatment, highlighting that different applications and target pollutants have considerably different plasma specification needs[17–19]. The incorporation of oxygen-containing functional groups, the opening of micropores, and the increment of surface roughness are all the results of the plasma treatment that are attributable to the enhancement in adsorption capacity[20,21]. Figure 2c showed that 0.1 M of $KMnO_4$, pre-treatment, significantly improved the adsorption capacity of plasma-treated ACF compared to concentrations ranging from 0.01 M to 1 M. This might be due to a lack of active sites available for surface oxidation to effectively produce enough reactive species to modify the ACF surface with MnO species[20,22]. Conversely, the excessive $KMnO_4$ concentrations can lead to redox reactions at the surface, potentially causing ACF structure dissolution or deterioration, resulting in loss of structural integrity, reduced surface area, and reduced adsorption capacity[23]. The optimum plasma parameters, which include 0.1 M $KMnO_4$, pre-treatment, 5 min of exposure duration, and 150 W of power, provide crucial results for effectively removing heavy metals.

Optical emission spectroscopy from the plasma sheath was used to identify prominent electroactive species involved in the surface modification of the ACF after MnO pre-treatment. According to Fig. 2d, atmospheric nitrogen, along with Ar and O_2, effectively embeds functional groups on carbon surfaces, indicating the creation of nitrogen-rich electroactive species in the plasma. The plasma-enhanced surface modification of the ACF is driven by the presence of singlet oxygen and the metastable Ar* species, which are primarily abundant in the plasma sheath, according to the OES spectra[24].

Mechanism of plasma reaction

Modified ACF undergoes a series of surface modification processes by plasma that enriches the material's surface and core with functional groups. The overall reaction mechanism is illustrated in Fig. 3. The first step is assumed to be (i) Formation of defects - The modified ACF structure experiences defects due to active plasma species, reactive oxygen and nitrogen species, free electrons, Frenkel-pair defects, and interstitial atom vacancies, enhancing its reactivity and surface characteristics, which are depicted in equations (2 to 5)[25,26]. Secondly, (ii)

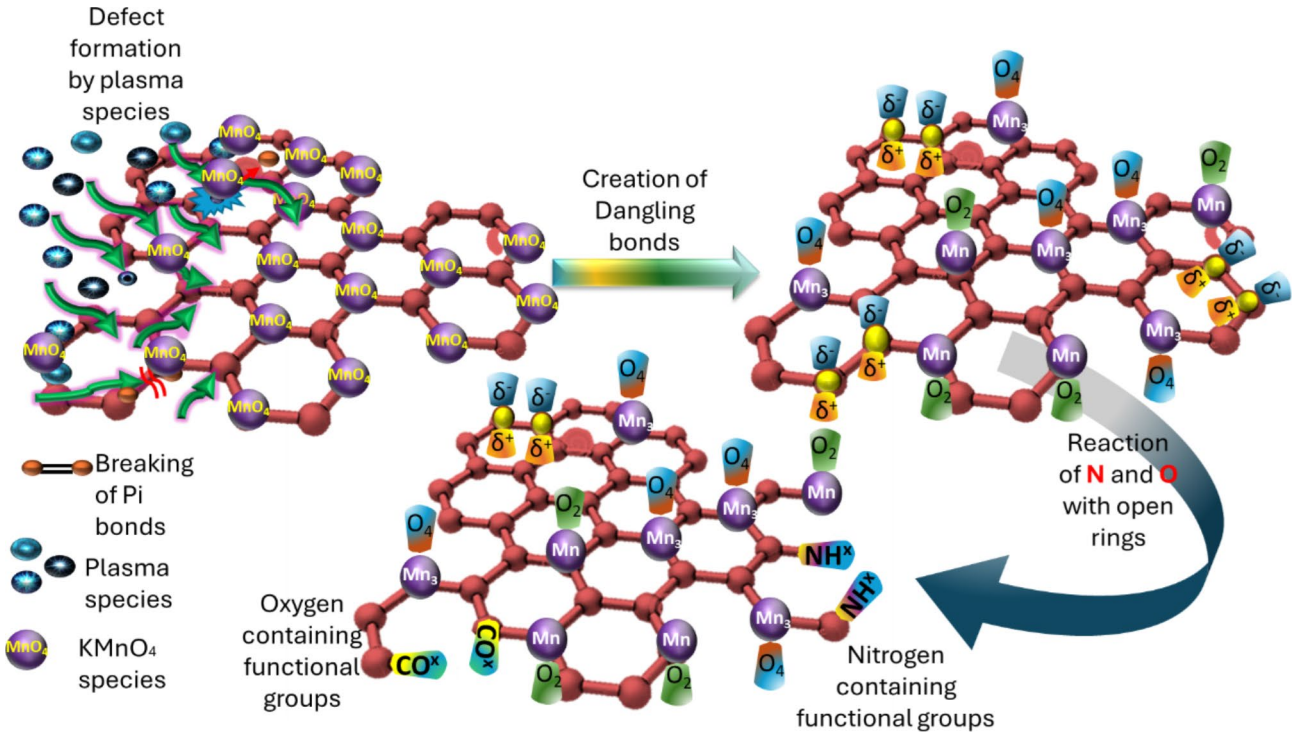

Fig. 3. Schematic anticipated illustration of the reaction of plasma species with ACF coated with MnO (modified ACF).

Breaking of π bonds - plasma treatment causes π bonds in modified ACF structure to rupture due to high energy electrons and reactive species, potentially creating new reactive sites on the modified ACF surface. Followed by (iii) Creation of dangling bonds and reduction of MnO species - Plasma treatment reduces MnO species on modified ACF surfaces to Mn_3O_4 and MnO_2, forming reactive sites and functional groups, resulting in increased dangling bonds[27]. These dangling bonds act as fresh sites for further reactions, as shown in equations (5 to 11). Finally, (iv) Creation of oxygen and nitrogen-containing functional groups - Plasma reactive species lead to the creation of oxygen-containing functional groups, such as hydroxyl (-OH) and carbonyl (-C=O), as well as nitrogen-containing functional groups, such as amine ($-NH_2$) and nitrile (-C≡N). The abundant MnO species on the modified ACF surface facilitate these reactions, further promoting the formation of Mn-based functional groups[28]. Plasma treatment and MnO pre-treatment coating activate oxidation, modifying ACF surface, producing functional groups, breaking π bonds, reducing MnO species, and introducing defects, improving ACF's reactivity and adsorption capability. Additionally, the equations from (2 to 11) are conjectured to comprehend the chemical processes that are taking place[10,29].

$$e^- + H_2O \rightarrow H^+ + 2\,OH^{\cdot} \quad (2)$$

$$Ar^+ + H_2O \rightarrow H_2O^+ + Ar \quad (3)$$

$$2\,OH^{\cdot} + O^{\cdot} \rightarrow H_2O_2 \quad (4)$$

$$3\,H_2O_2 + 3OH^{\cdot} \rightarrow Mn^{+2}/Mn^{+3} + 3\,OH_2^- + H_2O \quad (5)$$

$$MnO_4^- + 5e^- + 8H^+ \rightarrow Mn^{+2} + 4H_2O \quad (6)$$

$$MnO_4^- + 3e^- + 4H^+ \rightarrow MnO_2 + 2H_2O \quad (7)$$

$$MnO_4^- + e^- + OH^- \rightarrow MnO_4^{2-} \quad (8)$$

$$MnO_2 + Mn^{+2} + H_2O \rightarrow Mn_2O_3 + 2H^+ \quad (9)$$

$$MnO_2 + Mn^{+2} + 2H_2O \rightarrow Mn_3O_4 + 4H^+ \quad (10)$$

$$MnO_2 + Mn^{+2} + 2H_2O \rightarrow MnOOH + 2H^+ \quad (11)$$

Characterisations of plasma surface modified ACF

The X-ray Photoelectron Spectroscopy (XPS) analyses were conducted to discern structural and chemical modifications in Activated carbon felt (ACF), as presented in Fig. 4. Examination of survey peaks in Fig. 4a unequivocally indicates the successful origination of Mn peaks after the modification process[30]. A detailed

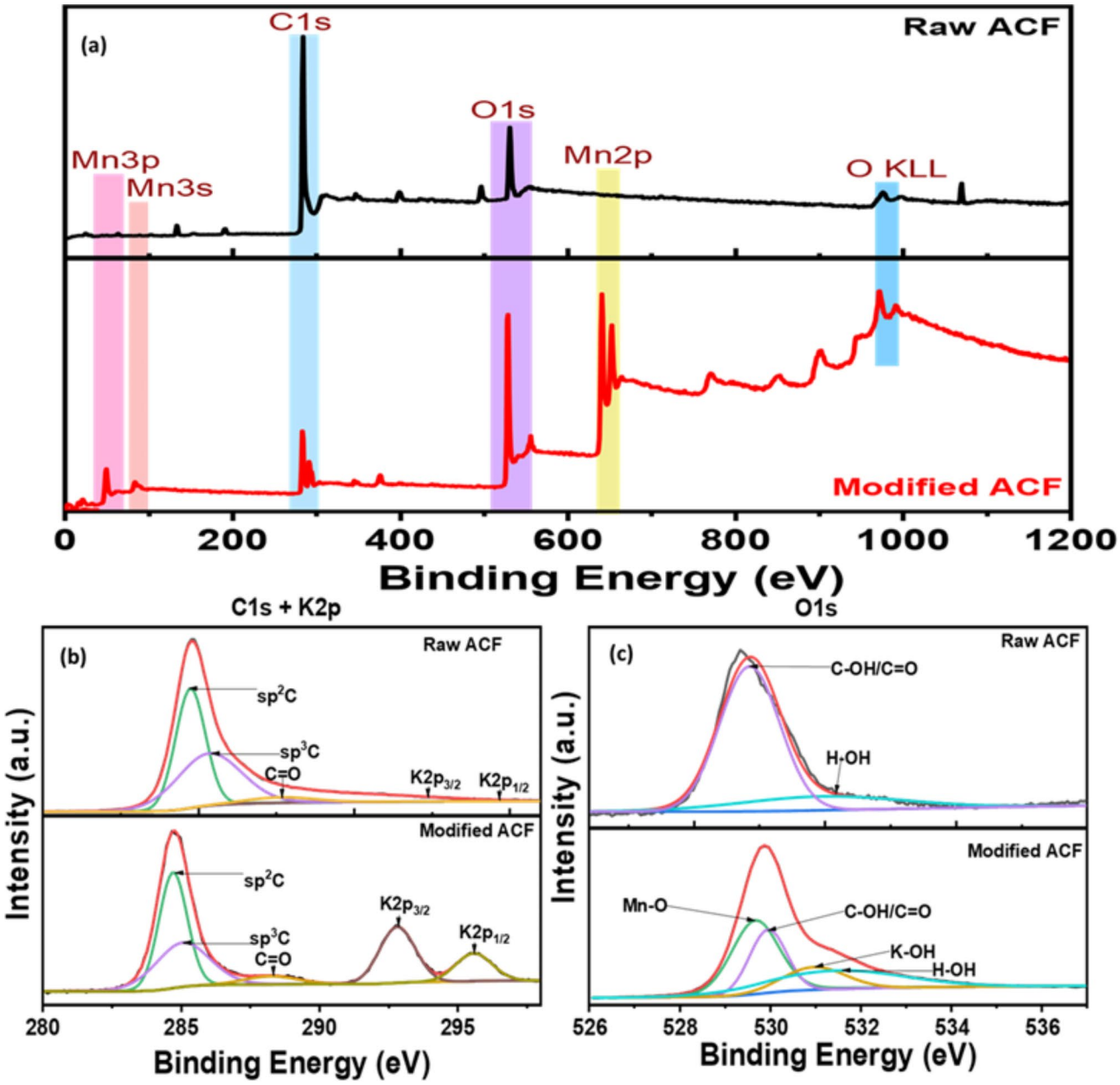

Fig. 4. XPS analysis of raw and modified ACFs (**a**) survey peaks of ACF before and after modification; deconvoluted peaks of (**b**) C1s + K2p; and (**c**) O1s.

deconvolution of C1s + K2p spectra unravelled intriguing insights. The emergence of K2p at ~ 292.85 eV and ~ 295.6 eV, accompanied by a relatively stronger peak area of C = O at ~ 287.7 eV, denotes a synergistic modification induced by $KMnO_4$, molecules and plasma treatment[31]. In Fig. 4b, the O1s spectra unveil compelling evidence of structural alterations. The appearance of additional peaks along with C-OH/C = O and H-OH for K-OH at ~ 531.0 eV and for Mn-O at ~ 529.7 eV substantiates the reduction of Mn species and the formation of new chemical species in the presence of plasma. These findings underscore the intricate interplay between $KMnO_4$ and plasma treatment, providing a nuanced understanding of the modifications occurring in ACF.

Furthermore, Fig. 5a shows the FTIR results for the modifications of adsorbent materials at various parameters. It was evident that the pre-treatment with MnO species and then plasma treatment had significant variations in the vibrational stretching of the functional groups on the adsorbent material. Notably, the FTIR spectrum exhibited intense peaks after plasma treatment in comparison to only MnO coating owing to the -OH group stretching vibrations that appeared in the range of 3800 – 3400 cm^{-1}, suggesting the introduction of hydroxyl (-OH) groups onto the adsorbent surface that was accredited to the improved adsorption of Cu(II) and Cd(II)[29]. Secondly, C = O stretching vibrations detected in the range of 2350 – 2200 cm^{-1} are allegedly responsible for increasing the adsorption capacity of the modified ACF and the C-O group[32]. The appearance of ester or etheric carbonyl group (C-O) vibrations in the region of 1800 – 1530 cm^{-1} was prominent evidence in the graph

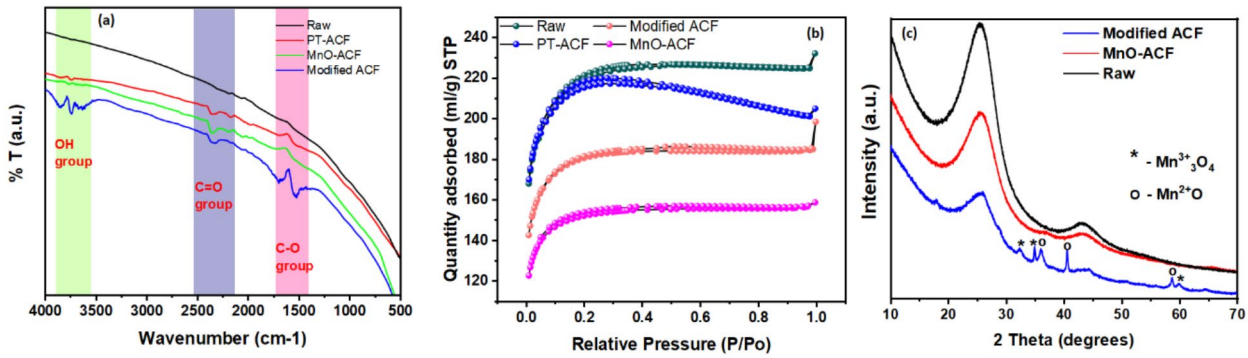

Fig. 5. Graphs of (**a**) FTIR spectra, (**b**) plots of BET surface adsorption and (**c**) XRD graph for ACF, MnO-ACF, and modified ACF.

indicating successful modification of the carbon skeleton structure of modified ACF by the addition of oxygen from the plasma species[33]. These findings suggest that the surface modification process involving MnO and plasma treatment has successfully introduced oxygen-rich functional groups such as hydroxyl, carbonyl, and ether/ester functional groups, making the material a promising candidate for boosted up adsorption of Cu(II) and Cd(II). Based on the data in Table S1, it is evident that atmospheric pressure plasma impacts the physical characteristics of adsorbents. The raw ACF was very porous in nature, with a surface area of 836.6 m^2/g; however, after plasma treatment, there was a small decrease in surface area, which can be ascribed to surface defects imparted by high-power collisional plasma molecules.

Furthermore, the MnO-ACF treated material was observed to reduce the highest amongst the group with a surface area of 588 m^2/g, which is suspected to be due to the clogged pores of the porous ACF material due to deposition of MnO particles. Lastly, the modified ACF had 692 m^2/g, indicating the clogged pores were exposed to high-power plasma particles, which resulted in more porous surface characteristics in the material. According to the IUPAC classification, the BET adsorption-desorption graph in Fig. 5b showed a pattern that resembled type II isotherm, which denotes multilayer adsorption that is reversible and suggests the presence of meso- and macropores in the adsorbent material[34]. Therefore, it is certain that the plasma treatment was quite efficient in increasing surface area, presumably because of the production of surface defects and new pores. On the other hand, the MnO pre-treatment, which involves a chemical reaction, reduced the surface area.

Combining pre-treatment with MnO and plasma treatments resulted in moderate surface area, with structural modifications examined through X-ray diffraction analysis. Referring to Fig. 5c, the XRD study showed no distinct crystalline Mn species peaks before plasma treatment and MnO coating, suggesting non-crystalline manganese species in the material, but significant changes were observed after plasma treatment. The reduction of the manganese species and subsequent generation of the Mn_3O_4 and MnO crystalline phases indicated the plasma treatment promoted the successful transformation of Mn species. The highly energetic characteristics of the plasma treatment process trigger a series of chemical reactions on the material surface, culminating in structural and functional changes[35]. The MnO coating significantly enhanced the reduction of manganese species in the modified ACF material, with plasma treatment playing a crucial role in initiating the redox process. The spectrum revealed six distinct peaks at $2\theta = 11.4°$, 21.4°, 25.4°, 31.5°, 35.7°, 41.3°, and 57.9°. The broad peak at 21.4° corresponds to amorphous carbon and the (101) reflection of tetragonal MnO_2, while the other five peaks are assigned to tetragonal MnO_2 (JCPDS reference card number 18–0802). These results align with previous research on the impact of plasma treatment on material properties[36]. Thus, conclusively, XRD analysis helps to gain valuable insights into the structural changes induced by the plasma treatment and MnO coating process, confirming the successful reduction and crystallisation of the Mn species.

The investigations conducted by FE-SEM showed invaluable insights into the morphological changes of the ACFs under various treatments. As seen in Fig. 6a,b, it can be observed that the surface of raw ACF exhibited a remarkably smooth surface, which revealed a pristine, unaltered structure characterised by a lack of surface irregularities. In the next stage, upon coating the ACF with MnO (MnO-ACF), there was a noteworthy transformation observed from the smooth surface coating; there was a smooth formation of spherical spheres onto the surface, as observed in Fig. 6c,d. The deposition of MnO significantly alters the surface chemistry of ACF, resulting in a distinct change in surface morphology after plasma treatment. Also, it was found that small pits and broken surfaces on modified ACF surfaces were due to plasma's disruptive effect, as shown in Fig. 6e,f. Pre-treatment with MnO and plasma resulted in significant modifications to the surface morphology of the fibre. As shown in Fig. S1, EDX mapping revealed the elemental composition of the treated fibre, confirming the presence of carbon (75.84%), nitrogen (4.78%), oxygen (11.39%), and manganese (7.98%). These changes highlight the impact of the pre-treatment on the material's surface properties[37]. Conclusively, these FE-SEM results underscore the dynamic changes in ACF morphology throughout the experimental process. The transformation from a smooth surface to the formation of evenly coated spherical spheres of MnO molecules that were exposed to the high-power disruptive effects of plasma resulted in the subsequent surface reduction of MnO_4 molecules, which reformed into oxygen-rich species within the surface layers.

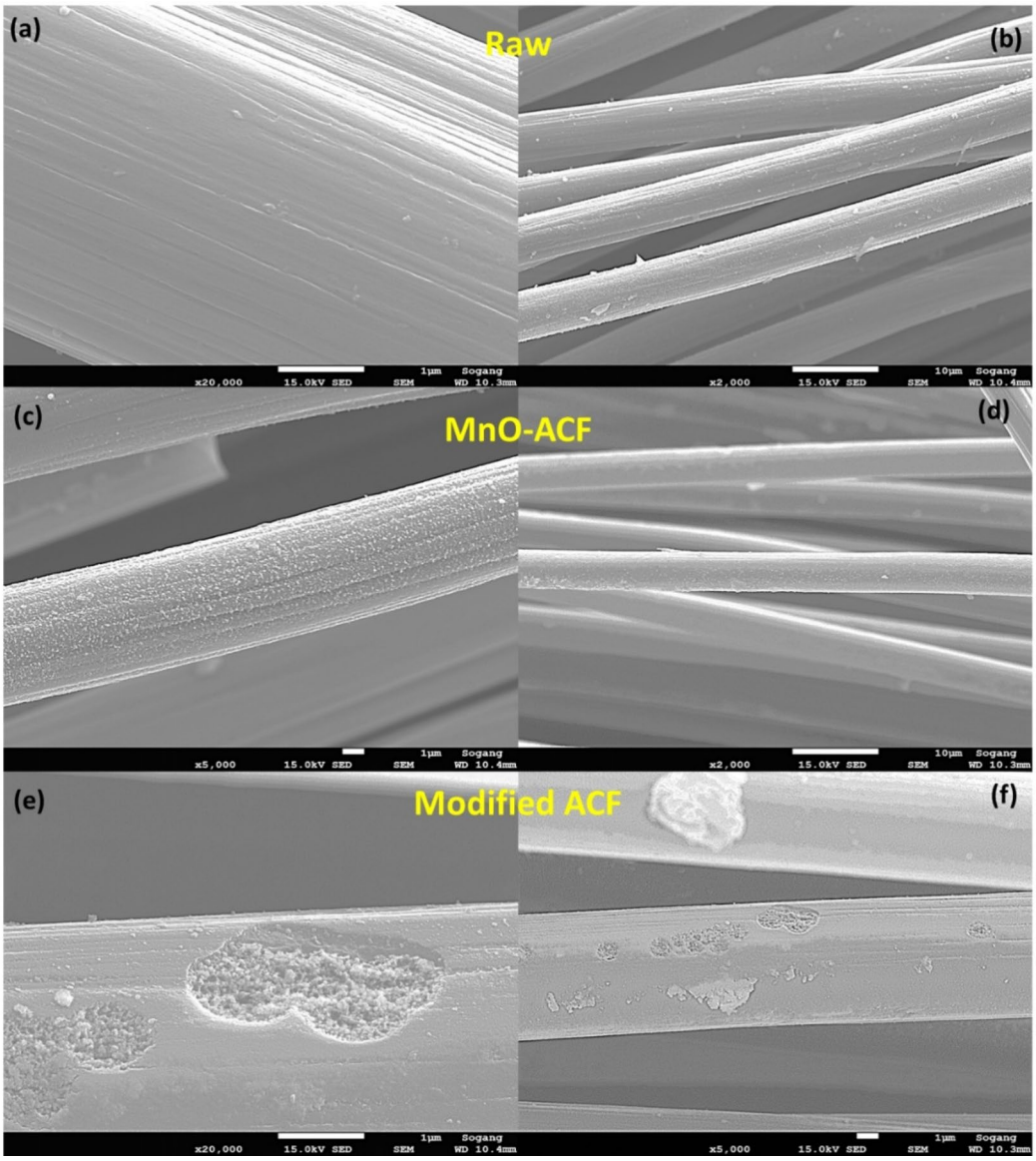

Fig. 6. SEM image of (**a**, **b**) raw ACF, (**c**, **d**) MnO ACF and (**e**, **f**) modified ACF.

Impact of pH

The impact of pH on the adsorption capabilities of Cu(II) and Cd(II) using modified ACF is depicted in Fig. 7a. The raw and modified ACF's pHzpc (zero-point charge) is shown in Fig. S2. After plasma surface modification, the modified ACF from pH 2 to pH 8 has a positive surface charge, which modulates ion exchange and electrostatic interaction[38,39]. pHzpc 8 facilitates species adsorption through both positive and negative surface charges, whereas between 4 and 6 pH, there is competition between protons and metal ions, increasing affinity for Cu(II) and Cd(II). Thus, pH 5 is optimal for metal removal due to abundant active sites created by oxygen-rich functional groups[1,38,40]. At pH levels above 5, precipitation dominates, reducing metal ion adherence to adsorbent.

Conversely, pH levels below 5 show intense competition between H^+ and Mn^{2+} species, reducing adsorption effectiveness. The electrostatic attraction between Cd(II)/Cu(II) and Mn^{2+} decreases surface positive charge, reducing metal repulsion. High solution pH strengthens this attraction, decreasing adsorption efficiency. In conclusion, pH greatly influences the optimal adsorption condition at pH 5, while lower and higher pH values lead to decreased efficiency due to competition with H^+ ions and metal ions and precipitation, respectively.

Contact time and initial concentration effect

Adsorption kinetics explain the solute's rate of adsorption as well as the adsorbates' duration of residence on the solid-liquid interface. These offer perceptions of the adsorption process's dynamics. Popular kinetic models are pseudo-first-order (PFO), pseudo-second-order (PSO), and Weber-Morris intraparticle diffusion (IPD)

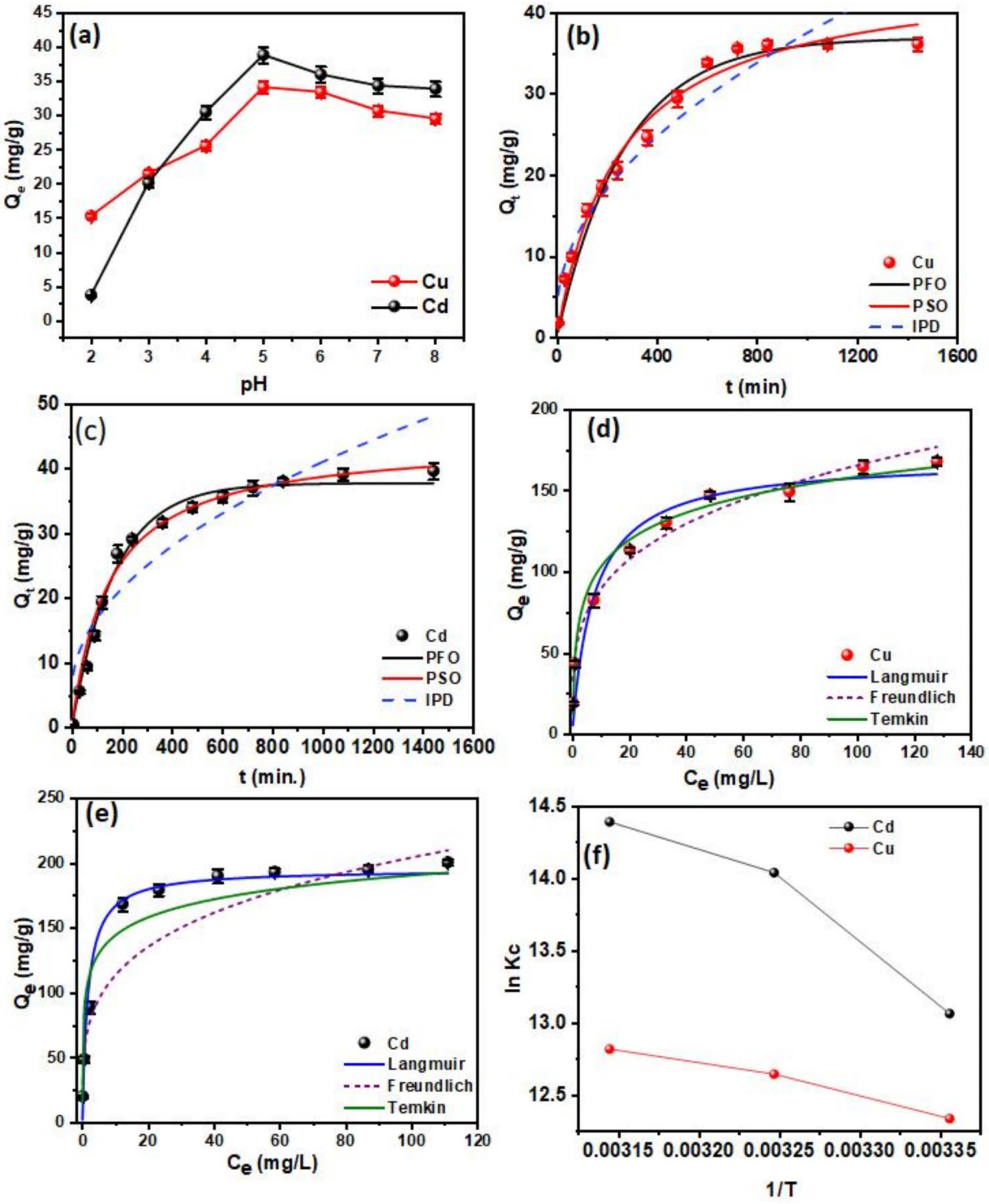

Fig. 7. Batch adsorption studies for 20 mg/L of Cu(II) and Cd(II) on 0.5 g/L dose of modified ACF for 720 min, pH 5, at 298 K respectively; (**a**) pH studies; (**b** and **c**) Contact time studies; and (**d** and **e**) Isotherm modelling plots between the concentrations of 10–200 mg/L (**f**) Vant-Hoff's plot.

models[39,41]. PFO implies that adsorption sites are occupied in proportion to empty sites, PSO chemisorption includes electron exchange, and the Weber-Morris intraparticle diffusion model looks at rate-limiting processes.

The adsorption kinetics for various ACF treatments are shown in Fig. S3. The most effective method involves sequential modification of $KMnO_4$, pre-treatment and plasma surface modification, while sole $KMnO_4$, dipping, or plasma treatment alone is less effective. The combined treatments ($KMnO_4$ + plasma) improve the adsorption

Metals	Q_e, exp (mg/g)	Pseudo-first order (PFO) $(Q_t) = Q_e(1-e^{o}-kt)$			Pseudo-second order (PSO) $(Q_t) = \frac{k_2 Q_e^2 t}{1+k_2 Q_e t}$			Weber-Morris (IPD) $(Q_t) = K_{id} t^{\frac{1}{2}} + C$		
		Q_e (mg/g)	k_1 (/min)	R^2	Q_e (mg/g)	K_2 (g/mg min)	R^2	k_{id} (mg/g)	C (mg/g)	R^2
Cd(II)	38.020	37.700	0.00592	0.9834	38.381	1.534E-4	0.9855	1.120	5.602	0.8268
Cu(II)	36.120	36.872	0.00371	0.9821	37.252	8.811E-5	0.9842	1.101	2.695	0.9282

Table 1. Kinetic parameters table used for metal ions adsorption onto modified ACF at a dosage of 0.5 g/L and pH 5.0 for Cu(II) and Cd(II) at 298 K. In this context, Q_e, exp and $Q_{e,\,TH}$ represent the experimentally and theoretically predicted equilibrium adsorption capacities of the metal ions (mg/g); k_1 and k_2 correspond to the PFO and PSO models, respectively, while R^2 denotes the correlation coefficient.

Metals	Langmuir $q_e = \frac{q_{max} b C_e}{1+bC_e}$			Freundlich $q_e = K_F + C_e^{\frac{1}{n}}$			Temkin $q_e = B ln(K_T) + B \ln(C_e)$		
	Q_{max} (mg/g)	K_L (L/mg)	R^2	K_F (mg/g) (L/mg)$^{1/n}$	n (L/g) (L/g)	R^2	K_T (L/mg)	B (J/mol)	R^2
Cd(II)	214.590	0.092	0.9850	38.521	2.700	0.9948	101.990	13.990	0.8933
Cu(II)	163.390	0.047	0.9681	18.268	2.267	0.9728	24.052	1.846	0.9780

Table 2. Brief description of isotherm models used for both metal ions adsorption onto modified ACF at a dosage of 0.5 g/L and pH 5.0 for Cu(II) and cd(II) at 298 K. Here, $C_e$denotes the metal ion concentration at equilibrium (mg/L); qe and qmax represent the equilibrium and maximum adsorption capacities of the metal ion (mg/g), respectively. The coefficients K_L, K_F, and $K_T$correspond to the Langmuir, Freundlich, and Temkin isotherm models, respectively. Parameter n is a constant that describes the linearity of the Freundlich adsorption isotherm related to the adsorption heat in the Temkin isotherm. Additionally, $R^2$is the correlation coefficient.

efficiency for Cu(II) and Cd(II) due to embedding functional groups on carbon surfaces, validating the dual-modification process for heavy metal removal in water remediation. Thus, Fig. 7b,c shows the results of an investigation into the adsorption kinetics of Cu(II) and Cd(II) onto modified ACF utilising different contact times. The study reveals the mechanisms of adsorption and the influence of Mn^{2+} ions on the adsorption process. The graph's trend shows that up until 600 min, the occupancy of the active adsorption sites grew; afterwards, it seemed to be gradually reaching equilibrium. Thus, the anticipated equilibrium time was fixed to be 720 min for further studies.

Furthermore, three models were employed to forecast the adsorption's kinetics. Cu(II) and Cd(II) adsorption on modified ACF was found to fit the pseudo-second-order (PSO) model, revealing a chemisorption process that contributes to the emergence of strong chemical interactions between the metal ions and the ACF external surface, as shown in Table 1. The obtained Q_e values are closely related to theoretical Q_e values, and the R^2 value is less than 1[41,42]. The Weber-Morris model of intraparticle diffusion (IPD) revealed the involvement of electron transfer and formation of stable bonds between modified ACF and contaminant metals, supporting the assumption that Mn^{2+} ions on the modified ACF surface can act as binding sites, promoting rapid chemisorption through the formation of complexes with metal ions[43,44]. Although the IPD model predicts that adsorption occurs mostly within the pores, the presence of Mn^{2+} ions provide more active sites and facilitates metal ion accessibility to the modified ACF intraparticle pores, enabling faster adsorption. This all indicates the creation of strong bonds during the chemisorption process due to the Mn^{2+} ions, which contributes to a better removal efficiency of Cd(II) and Cu(II)[38,40,45,46]. The adsorption process is further aided by the rapid intraparticle diffusion within the modified ACF, which allows efficient usage of the surface area available. Conclusively, the findings of this investigation amply validate that the adsorption of Cu(II) and Cd(II) onto modified ACF conforms to the pseudo-second-order model, signifying chemisorption accompanied by the creation of strong bonds. The presence of Mn^{2+} ions on the modified ACF surface serves as active binding that promotes access within the intraparticle pores, enhancing adsorption through intraparticle diffusion, as confirmed by the IPD model.

Figure 7d, e reveals essential adsorption isotherms that determine interactions between adsorbent and adsorbate, optimal adsorption capacity, and molecule distribution. Common models are Langmuir, Freundlich, and Temkin isotherms[47,48]. The Langmuir model assumes monolayer adsorption on a surface with identical sites, leading to a hyperbolic isotherm. The Freundlich model describes adsorption on heterogeneous surfaces with varying affinities, resulting in a logarithmic isotherm. The Temkin model accounts for interactions between adsorbate and adsorbent, assuming a linear decrease in the heat of adsorption with coverage, resulting in a linear isotherm at moderate concentrations[49].

Table 2 shows that the Q_{max} maximum adsorption capacities of Cu(II) and Cd(II) on modified ACF were 163.39 and 214.59 mg/g, respectively. The study reveals substantial metal ion adsorption capacity, with Mn^{2+} species creating more active sites for binding, following the Langmuir model, but with potential heterogeneity

and secondary forces. The modified ACF surface may have influenced adsorption, but reduced R^2 values suggest adsorption heterogeneity. The Langmuir model fits experimental data, while Freundlich predicts favourable adsorption[50].

The Temkin isotherm model reveals surface heterogeneity and energetics of the adsorption process. The equilibrium binding constants (K_T (L/mg)) for Cu(II) and Cd(II) were 24.05 and 101.99 respectively, indicating the modified ACF's significant affinity for the metal ions. The parameter B (J/mol), representing heat of adsorption, was 13.99 for Cd(II) and 1.846 for Cu(II), suggesting different levels of adsorption strength. These findings support the assumptions of the Temkin model, which reasonably describes the adsorption process for both metal ions on the modified ACF. The Langmuir and Temkin adsorption models explain adsorption behaviour but are not as effective as the Freundlich models in modifying ACF's diverse adsorption affinity[51]. Recent studies on the adsorption of Cu(II) and Cd(II) from aqueous solutions have investigated various adsorbents, as summarised in Table 3. Among them, the modified ACF exhibits heterogeneous adsorption affinity due to its diverse functional groups. This characteristic highlights its versatility in removing heavy metals, particularly Cu(II) and Cd(II), under varying pH and dosage conditions.

Thermodynamical aspect of adsorption

The thermodynamics of the adsorption process for Cu(II) and Cd(II) utilising modified ACF were investigated and are plotted in Fig. 7f using the standard Gibbs free energy change (G°), enthalpy change (H°), and entropy change (S°), insights into spontaneity, heat effects, and change in disorderliness with rising temperature were assessed. The thermodynamic parameters for Cd(II) and Cu(II) adsorption on modified ACF were calculated and shown in Table S2. ΔG° values ranged from − 32.35 to -38.04 kJ/mol for Cd(II) and from − 30.55 to -33.88 kJ/mol for Cu(II). The negative values indicate spontaneous adsorption, supported by similar findings with MnO_2 and the presence of active sites, including the Mn^{2+} ions, on the ACF surface, enhancing metal ion binding[52,53].

The positive ΔH° values of 52.64 kJ/mol and 19.02 kJ/mol for Cd(II) and Cu(II) respectively, on modified ACF indicate an endothermic process where environmental energy is involved[54,55]. Heat energy overcomes energy barriers, and Mn^{2+} ions enhance strong bond formation and chemisorption, contributing to the reaction's endothermic nature. Adsorption onto modified ACF shows an increase in disorder, indicated by positive ΔS° values for the Cd(II) = 286.03 J/K.mol and Cu(II) = 166.53 J/K.mol. Various mechanisms, including chemisorption and complex formation, contribute to this disorder. Positive ΔS° readings demonstrate increased entropy, resulting from faster movement of Cu(II) and Cd(II) ions at higher temperatures. This implies higher mobility and entropy during adsorption[51].

Co-existing ions studies

The influence of various ions on Cu(II) and Cd(II) adsorption onto modified ACF was investigated. Specifically, the influence of cationic groups (potassium, calcium, magnesium, and sodium) and anionic groups (nitrates, sulfates, phosphates, and chlorides) on the adsorption efficiency of Cu(II) and Cd(II) was scrutinised. Anionic co-existing species impacted the removal of Cu(II) and Cd(II), as shown in Fig. S4a, b. Anionic species, particularly phosphates, negatively affected the adsorption of Cu(II) and Cd(II). The negative charge of phosphate groups can form complexes with metal ions, reducing their availability to bind to active sites on the modified ACF surface. As shown in Fig. S4c,d, different cations negatively affected adsorption. Mg(II) and Ca(II) had a greater impact on Cd(II) adsorption than Cu(II). Magnesium and calcium, divalent cations, compete with negatively charged surfaces for adsorption sites, inhibiting Cd(II) adsorption. Their higher charge density reduces electrostatic attraction, resulting in lower adsorption capacity[10]. The results emphasise the significance of the presence of phosphate groups and divalent cations, particularly Mg(II) and Ca(II), which have a substantial implication on the efficiency of adsorption by decreasing the number of available adsorption sites and interfering with the

Metal ions	Adsorbents	Q_{max} (mg/g)	Conditions [pH & dosage (g/L)]	Ref.
Cd(II)	AC-thiourea	12.10	7 & 0.5	13
	EO ACC	157.34	7.5 & 0.5	50
	CMOF-199	113.30	5 &0.75	51
	MBC	54.70	6 & 2.0	52
	P/Mg-engineered biochars	113.90	5.6 & 4.0	53
	ZIF − 8@PAN nanofiber	102.00	7.5 & 0.4	54
	Modified ACF	214.59	5 & 0.5	This study
Cu(II)	PTh/MnO_2	60.79	6 & 2.0	55
	NM-ACFF	23.13	6 & 0.2	26
	IDA-OAC	84.51	5 & 0.02	56
	Fe_3O_4-MnO_2-EDTA	46.39	6 &0.2	57
	SA/CMC-ZFN	63.29	5 & 0.5	58
	Modified ACF	163.39	5 & 0.5	This study

Table 3. Literature reports on extensive comparison of the adsorption capacities (Q_e) for Cu(II) and Cd(II) using various adsorbents.

electrostatic interaction between the metal ions and the surface of the modified ACF, thereby influencing the adsorption process of Cu(II) and Cd(II).

Regeneration and recyclability studies

Traditional methods like rotation and centrifugation have limitations in mass transfer during recycling processes. Sonication offers faster transfer, efficient reactions, and improved dispersion, accelerating recycling studies[56]. Thus, regeneration of adsorbed sites of modified ACF through sonication was used for effective adsorption. The study yielded results shown in Fig. S4e–f pointing that regeneration can be achieved by sonicating 3% nitric acid and rinsing with distilled water, restoring adsorption sites on modified ACF, and accelerating metal ion removal by disrupting adsorbed species and facilitating their release from the ACF matrix[57]. Figure S4f shows the test results for different time intervals. Thus, 15 min of sonochemical disruption effectively regenerated and desorbed Cu(II) and Cd(II) ions from modified ACF[58]. As observed from Fig. S5, the modified ACF was washed with distilled water to neutralise the pH and ensure optimal adsorption performance for over 5 cycles[59]. Efficient desorption of Cu(II) and Cd(II) ions reveals the potential for continuous adsorption-desorption cycles, increasing sustainability and cost-effectiveness. This study concludes that with 3% nitric acid, sonication, and washing, the modified ACF can be reused for up to 5 cycles by breaking metal adsorbate bonds and releasing Cu(II) and Cd(II) from the surface.

Column studies

To assess breakthrough performance, the modified ACF's adsorption capability was tested using three models (Thomas, Adams-Bohart, and Yoon-Nelson). The Thomas model was used to analyse the breakthrough curves during adsorption. Fig. S5a,b shows a strong fit and provides insights into equilibrium-driven processes and adsorption kinetics. Table 4 presents important parameters: rate constant (K_{Th}) for Cd(II) was 0.023 and for Cu(II) was 0.0220 (L/mg.day), and adsorption capacity (Q_{Th}) for Cd(II) was 0.217 mg/g and for Cu(II) was 0.233 mg/g. The Thomas model confirms the reversible nature of the adsorption process and accurately assesses the adsorption performance of the modified ACF in the column configuration without axial dispersion[60].

As seen in Fig. 8a,b, the Thomas model showed that the adsorbate's adsorption process depended on initial concentration, contradicting the Adams-Bohart model. This suggests that factors other than adsorbent concentration and capacity control the adsorbent rate. Additionally, the Yoon-Nelson model revealed information about the interaction between the adsorbate and adsorbent, including internal and external mass transfers[61]. Fitting this model to breakthrough curves provided insights into the dynamic behaviour of the adsorption process.

The 50% breakthrough time for adsorption was found to be 46 days and 51 days for Cd(II). and Cu(II), respectively. Table 4 presents the data of the breakthrough curve evaluation indicated by the equation variable and the sum square error for each model. Thomas and Yoon's models showed excellent agreement with theoretical values, which were validated by low error levels[62,63]. Plasma treatment enhances the adsorption efficiency of ACF by increasing surface area and introducing functional groups, allowing selective adsorption of contaminants like Cu(II) and Cd(II). Plasma treatment is an environmentally friendly, cost-effective, and sustainable alternative to traditional hazardous chemicals, potentially leading to advancements in adsorption technology.

Characterisations for after adsorption of Cu(II) and cd(II)

Figure 8c shows a decrease in peak intensity of Mn^{3+} and Mn^{2+} after adsorption of Cu(II) and Cd(II), indicating their role in the adsorption process. MnO coating on ACF substrate confirmed by XRD analysis, demonstrating adhesion of Mn species[45]. The FE-SEM analysis shown in Fig. 8d–e elucidated prominent surface changes on the ACF after adsorption. Images of the modified ACF treated with MnO-PT revealed a relatively homogeneously coated layer of MnO and pits filled with MnO_2. Figure 8f–i indicates the formation of solid scales on the surface, indicating a complex interaction between the modified ACF and Cu(II) and Cd(II) ions. These scales affect solution pH during adsorption, causing chemisorption or surface precipitation. Modified ACF surface exhibits metal oxide precipitation, phase transition, and co-precipitation, enhancing adsorption capacity.

The XPS survey peaks in Fig. 9a present several key findings. The peaks of Cu(II) and Cd(II) confirm the successful binding of heavy metals to the modified ACF. The peaks of Mn3p, Mn3s, Mn2p, C1s, and O1s also

		Thomas $Ln\left(\frac{C_0}{C_t}-1\right)=\frac{K_{TH}Q_{TH}m}{Q}-K_{TH}C_0t$			Adams-Bohart $Ln\left(\frac{C_t}{C_0}\right)=K_{AB}C_0t-K_{AB}N_0\left(\frac{Z}{U_0}\right)$			Yoon-Nelson $Ln\left(\frac{C_t}{C_0-C_t}\right)=K_{YN}t-\tau K_{YN}$		
Metals	C_0 (mg/L)	K_{TH} (L/mg day)	Q_{TH} (mg/g)	R^2	K_{AB} (L/mg day)	N_0 (mg/cm^3)	R^2	K_{YN} (/min)	τ (day)	R^2
Cd(II)	5.189	0.023	0.217	0.933	6.691E-09	15.609	0.915	0.000084	46	0.927
Cu(II)	4.768	0.020	0.233	0.896	6.117E-09	15.173	0.824	0.000064	51	0.896

Table 4. Column studies of Cu(II) and Cd(II) ions on modified ACF for breakthrough adsorption capacities and model parameters. (C_t and C_0 = Concentrations of the adsorbate in the outlet and in the inlet, respectively; K_{TH}= Thomas constant; Q_{TH}= maximum adsorption capacity (mg/g); m = mass of the adsorbent (g); K_{AB}= Adam-Bohart's constant, N_0 = adsorption capacity of the adsorbent per unit volume of the bed, Z = bed height; U_0 = superficial velocity; t = operating time; τ = breakthrough time; K_{YN}= Yoon-Nelson's constant)

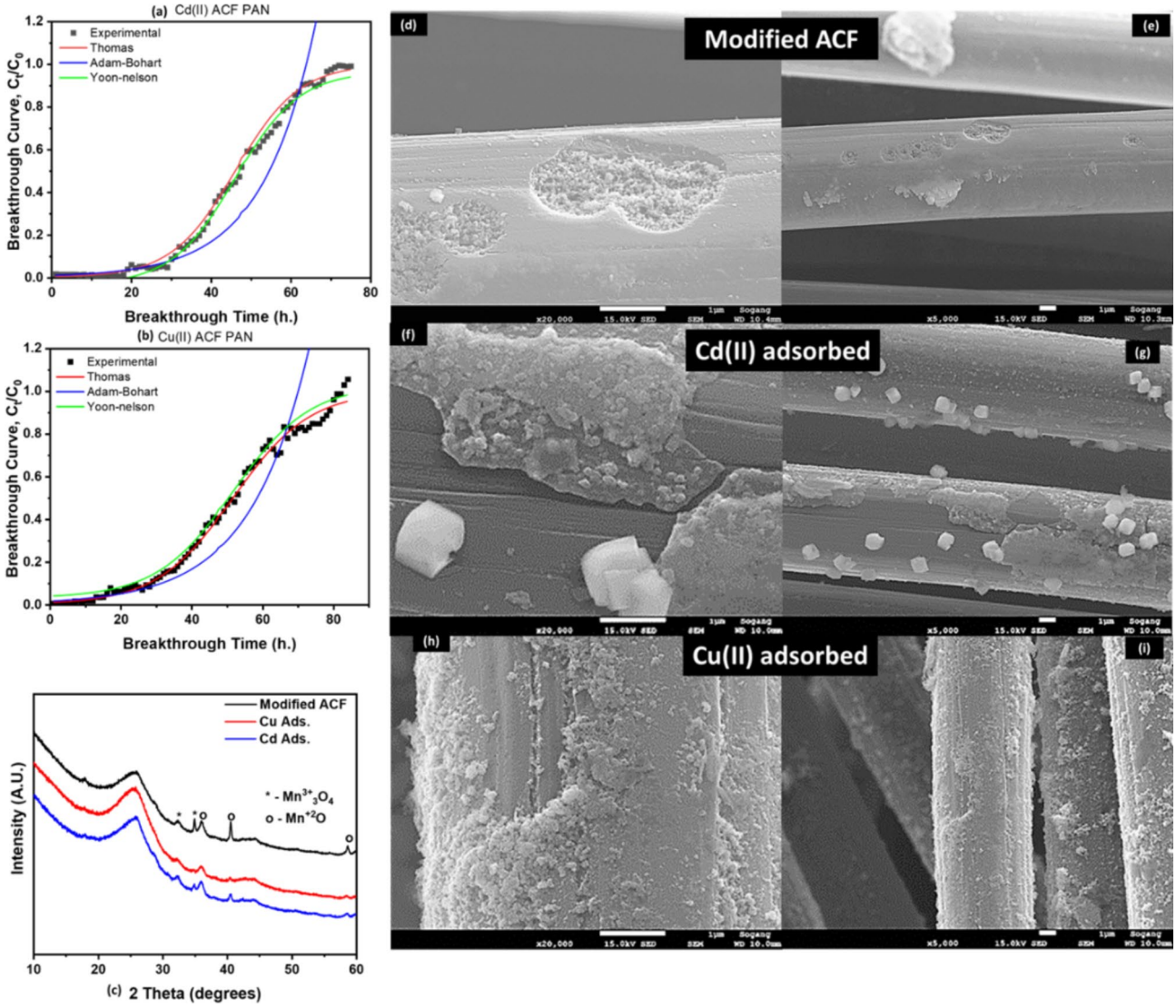

Fig. 8. (**a** and **b**) Column modelling data; after adsorption graphs (**c**) XRD analysis (**d**–**i**) FE-SEM images of Cd(II) and Cu(II) onto modified ACF respectively.

indicate the involvement of these elements in the adsorption process. Deconvolution of the C1s + K2p spectra in Fig. 9b reveals sharp peaks at ~ 284 eV sp^2C and ~ 285 eV sp^3C, suggesting different carbon states. The peak at ~ 287 eV indicates the presence of C = O, while the peaks at ~ 293-296 eV confirm the presence of potassium (K) from $KMnO_4$, which reduces after adsorption. The C1s spectral peaks show a decrease in the functional groups C = O and sp^2C, indicating their involvement in chemical adsorption. In the case of Cu(II) adsorption, hydroxide formation suggests the precipitation of $Cu(OH)_2$, aligning with surface complexation. Deconvolution of the O1s spectra in Fig. 9c shows distinct peaks corresponding to various oxygen-containing functional groups, including Mn-O, Mn-OH, K-OH, and H-OH. The increased peak areas of Mn-O, Mn-OH, K-OH, and H-OH after Cd(II) and Cu(II) adsorption indicate the involvement of Mn and K species, as well as hydroxyl groups, in enhancing the adsorption capacity[30]. Figure 9d reveals the dominance of Mn^{+4} and Mn^{2+} states in the adsorption process. Overall, the adsorption mechanism involves sp^2C, C = O, Mn^{+4}, and Mn^{2+} in surface complexation and precipitation. Conclusively, Fig. 10 represents the adsorption mechanism of Cu(II) and Cd(II) onto the modified ACF, which is suggested to entail a complex interplay of ion exchange, co-precipitation, H-bonding, and complexation processes. This is corroborated by the high Q_{max} values, extended equilibrium time, and active involvement of MnO and oxygen-rich species observed in the XPS, XRD, and FE-SEM analyses[64].

Conclusions

In this study, plasma treatment combined with a 0.1 M $KMnO_4$ coating significantly enhances the adsorption efficiency of modified ACF for heavy metals, offering improvements in surface properties with MnO-active and oxygen-rich species. The synergistic effect of plasma and $KMnO_4$, pre-treatment markedly boosts the removal of Cd(II) and Cu(II), presenting plasma treatment as an eco-friendly alternative to hazardous chemical

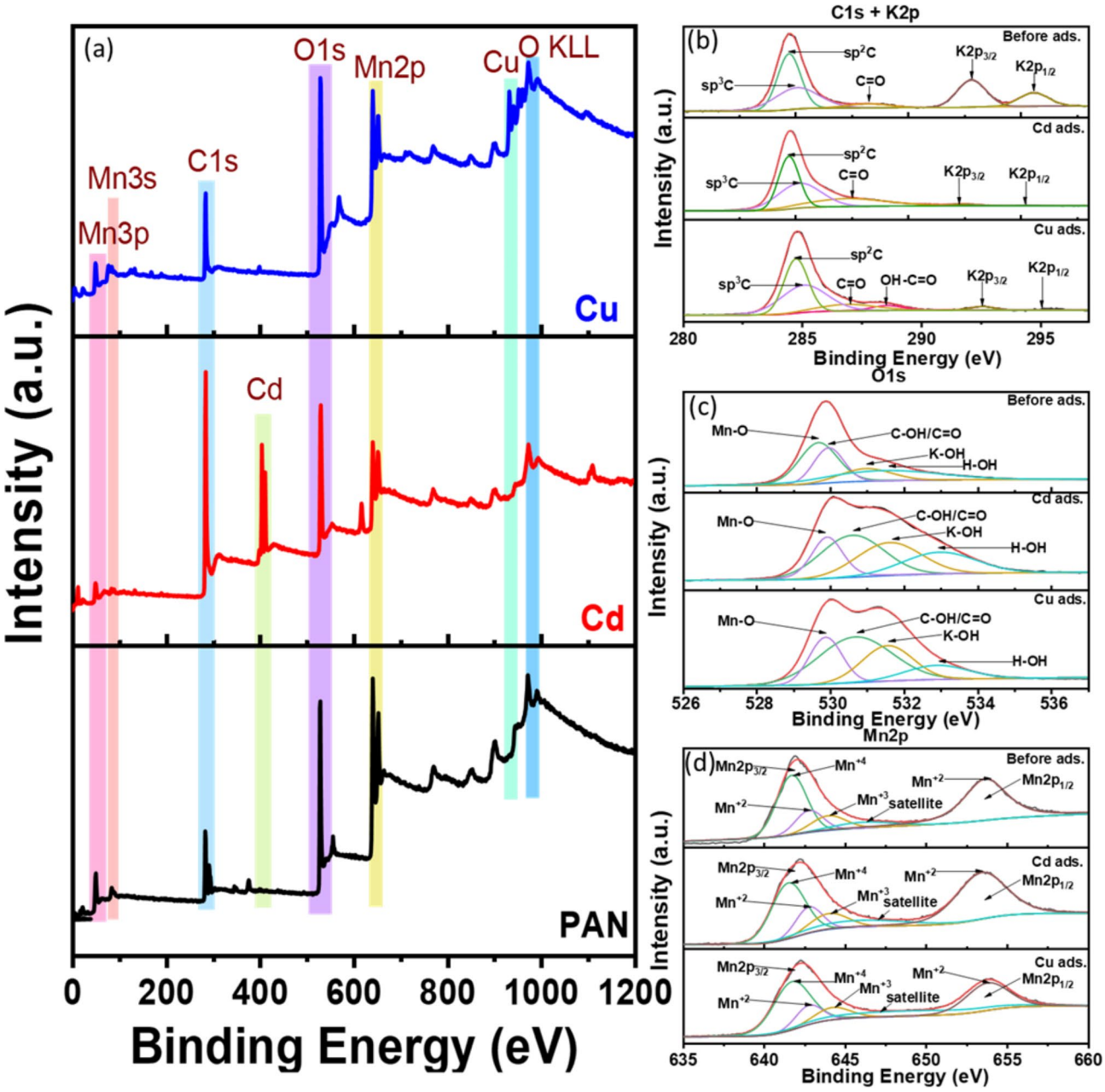

Fig. 9. XPS analysis of modified ACF (**a**) survey peaks of modified ACF before and after adsorption of Cu(II) and Cd(II); deconvoluted peaks of (**b**) C1s + K 2p; (**c**) O1s and (**d**) Mn 2p.

modifications. The adsorption kinetics and isotherm experiments reveal high capacities (Q_{max}) for Cu(II) (163.39 mg/g) and Cd(II) (214.59 mg/g), involving complex mechanisms such as complexation, ion exchange, and co-precipitation. While the modified ACFs are effective for heavy metal removal, their performance decreases in the presence of phosphates and divalent cations but maintains over 60% efficiency after five recycling cycles, suggesting potential for long-term use. Compared to related studies, this work provides a more comprehensive understanding of surface modification mechanisms and demonstrates the synergistic benefits of combining plasma treatment with $KMnO_4$, which enhances both performance and sustainability. Future studies can be focused on optimising treatment parameters and further investigating the long-term stability and regeneration capabilities of the modified ACFs under various environmental conditions.

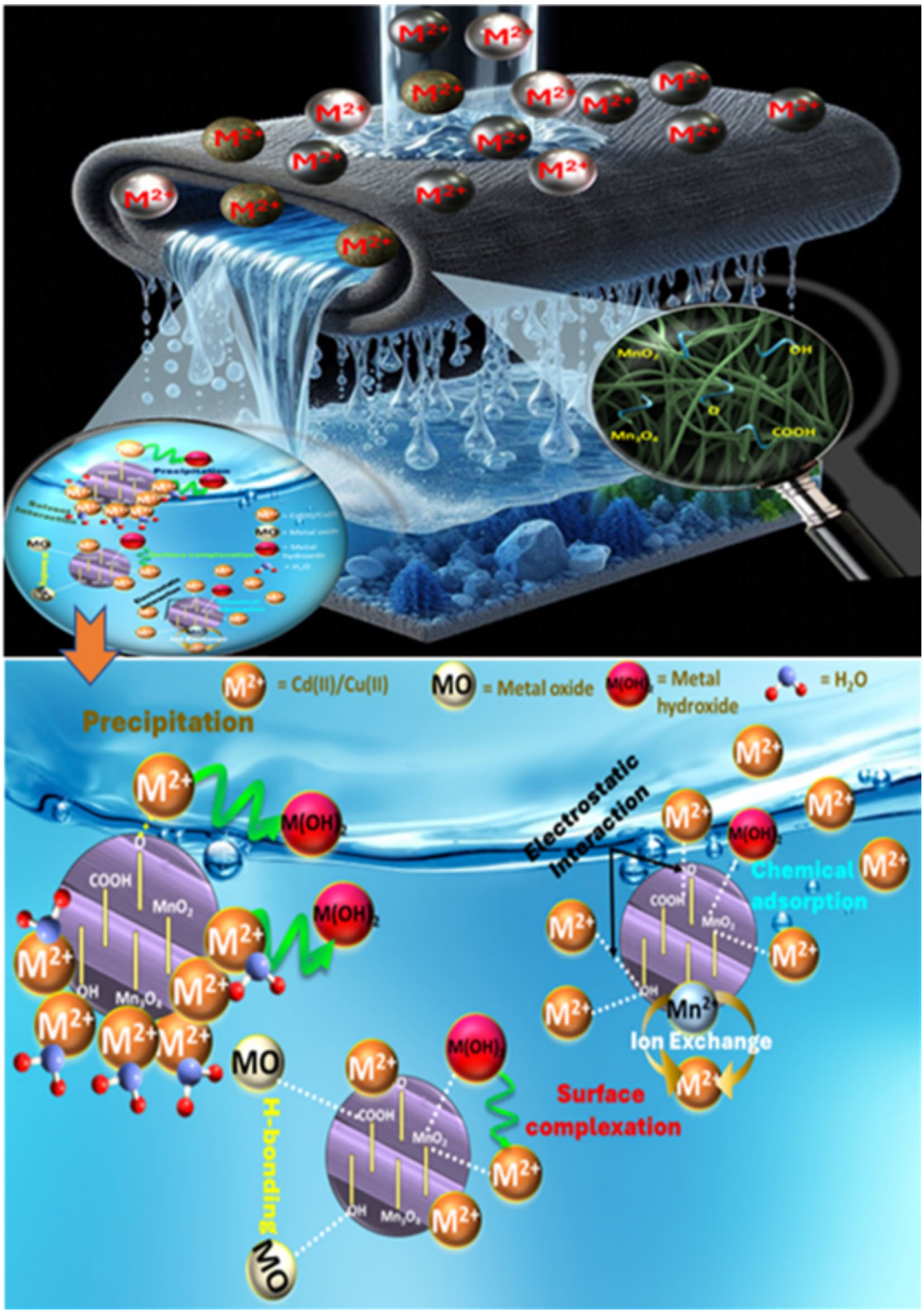

Fig. 10. Anticipated Cu(II) and Cd(II) adsorption mechanism onto modified ACF.

Data availability

The datasets used and analysed during the current study are available from the corresponding author (Prof. Janardhan Reddy Koduru) on a reasonable request.

Received: 2 November 2024; Accepted: 27 December 2024
Published online: 06 January 2025

References

1. Djati Utomo, H. & Hunter, K. A. Adsorption of divalent copper, zinc, cadmium and lead ions from aqueous solution by waste tea and coffee adsorbents. *Environ. Technol.* **27**, 25–32 (2006).
2. Lingamdinne, L. P., Lebaka, V. R., Koduru, J. R. & Chang, Y. Y. Insights into manganese ferrite anchored graphene oxide to remove cd(II) and U(VI) via batch and semi-batch columns and its potential antibacterial applications. *Chemosphere* **310**, 136888 (2023).
3. Lingamdinne, L. P. et al. Insights into kinetics, thermodynamics, and mechanisms of chemically activated sunflower stem biochar for removal of phenol and bisphenol-A from wastewater. *Sci. Rep.* **14**, 1–13 (2024).
4. Samanth, A., Vinayagam, R., Varadavenkatesan, T. & Selvaraj, R. Fixed bed column adsorption systems to remove 2,4-dichlorophenoxyacetic acid herbicide from aqueous solutions using magnetic activated carbon. *Environ. Res.* **261**, 119696 (2024).
5. Selvaraj, R. et al. Modeling 2,4-dichlorophenoxyacetic acid adsorption on candle bush pod-derived activated carbon: Insights from advanced statistical physics models. *J. Water Process. Eng.* **66**, 106027 (2024).
6. Liu, Q. X. et al. Adsorption of methylene blue from aqueous solution onto viscose-based activated carbon fiber felts: Kinetics and equilibrium studies. *Adsorpt. Sci. Technol.* **37**, 312–332 (2019).
7. Angaru, G. K. R. et al. Facile synthesis of economical feasible fly ash–based zeolite–supported nano zerovalent iron and nickel bimetallic composite for the potential removal of heavy metals from industrial effluents. *Chemosphere* **267**, 128889 (2021).
8. Zhang, H. et al. Enhanced removal of heavy metal ions from aqueous solution using manganese dioxide-loaded biochar: Behavior and mechanism. *Sci. Rep.* **10** (1), 10–11 (2020). (2020).
9. Momin, Z. H., Angaru, G. K. R., Lingamdinne, L. P., Koduru, J. R. & Chang, Y. Highly efficient cd(II) removal from groundwater utilising layered mixed metal oxides-graphitic carbon nitride composite with improved cycling stability. *J. Water Process. Eng.* **56**, 104276 (2023).
10. Pal, C. A. et al. Plasma-modified viscose rayon activated carbon felt (VR-ACF) for Cu(II) and cd(II) decontamination-mechanism and continuous-flow column operation. *Chem. Eng. J.* **496,** 154331. https://doi.org/10.1016/J.CEJ.2024.154331 (2024).
11. Rajumon, R., Aravind, S. P., Bhuvaneshwari, S., Ranjitha, J. & Mohanraj, P. Removal of cadmium heavy metal ions from wastewater by electrosorption using modified activated carbon felt electrodes. *Water Sci. Technol.* **82**, 1430–1444 (2020).
12. Li, X., Hu, Y., She, D. & Shen, W. B. Modified activated carbon fiber felt for the electrosorption of norfloxacin in aqueous solution. *Sustain. (Switzerland)* **12**, 3986 (2020).
13. Shenton, M. J. & Stevens, G. C. Surface modification of polymer surfaces: atmospheric plasma versus vacuum plasma treatments. *J. Phys. D Appl. Phys.* **34**, 2761 (2001).
14. Gupta, V. K. et al. Study on the removal of heavy metal ions from industry waste by carbon nanotubes: Effect of the surface modification: A review. *Crit. Rev. Environ. Sci. Technol.* **46**, 93–118 (2016).
15. Elammari, F. A. & Daniels, S. Polymer surface modification using Atmospheric pressure plasma. *Encyclopedia Materials: Plast. Polym.* **1–4**, 575–590 (2022).
16. Chu, G. et al. Evolution of surface morphology and properties of diamond films by hydrogen plasma etching. *Green. Process. Synthesis* **12**, 20228110 (2023).
17. Bai, B. C., Lee, H. U., Lee, C. W., Lee, Y. S. & Im, J. S. N2 plasma treatment on activated carbon fibers for toxic gas removal: Mechanism study by electrochemical investigation. *Chem. Eng. J.* **306**, 260–268 (2016).
18. Okajima, K., Ohta, K. & Sudoh, M. Capacitance behavior of activated carbon fibers with oxygen-plasma treatment. *Electrochim. Acta*. **50**, 2227–2231 (2005).
19. Sun, X. et al. Advance in using plasma technology for modification or fabrication of Carbon-based materials and their applications in environmental, material, and energy fields. *Adv. Funct. Mater.* **31**, 2006287 (2021).
20. Qiu, C., Jiang, L., Gao, Y. & Sheng, L. Effects of oxygen-containing functional groups on carbon materials in supercapacitors: A review. *Mater. Des.* **230**, 111952 (2023).
21. Xiao, J. et al. Rapid and continuous atmospheric plasma surface modification of PAN-based carbon fibers. *ACS Omega*. **7**, 10963–10969 (2022).
22. Yang, H. et al. Oxidation path analysis of NO in the adsorption and removal process using activated carbon fibers. *J. Fuel Chem. Technol.* **40**, 1002–1008 (2012).
23. Wang, X. et al. Key factors and primary modification methods of activated carbon and their application in adsorption of carbon-based gases: A review. *Chemosphere* **287**, 131995 (2022).
24. Adhikari, B. C., Lamichhane, P., Lim, J. S., Nguyen, L. N. & Choi, E. H. Generation of reactive species by naturally sucked air in the Ar plasma jet. *Results Phys.* **30**, 104863 (2021).
25. Akdoğan, E. & Şirin, H. T. Plasma surface modification strategies for the preparation of antibacterial biomaterials: A review of the recent literature. *Mater. Sci. Eng.: C.* **131**, 112474 (2021).
26. Şahin, Ö., Kaya, M. & Saka, C. Plasma-surface modification on bentonite clay to improve the performance of adsorption of methylene blue. *Appl. Clay Sci.* **116–117**, 46–53 (2015).
27. Dorai, R. & Kushner, M. J. Plasma surface modification of polymers using atmospheric pressure discharges. *IEEE Int. Conf. Plasma Sci.* **329** https://doi.org/10.1109/PLASMA.2002.1030666 (2002).
28. Qiao, Y. et al. Plasma surface modification coupled with thermal and step-over distance effects on significant fracture improvement of adhesively-bonded metal-CFRTP dissimilar materials. *Compos. Sci. Technol.* **232**, 109833 (2023).
29. Ortiz-Ortega, E., Hosseini, S., Martinez-Chapa, S. O. & Madou, M. J. Aging of plasma-activated carbon surfaces: Challenges and opportunities. *Appl. Surf. Sci.* **565**, 150362 (2021).
30. Barai, H. R., Banerjee, A. N. & Joo, S. W. Improved electrochemical properties of highly porous amorphous manganese oxide nanoparticles with crystalline edges for superior supercapacitors. *J. Ind. Eng. Chem.* **56**, 212–224 (2017).
31. Wu, Z. G. et al. Synthesis of a novel tunnel Na0.5K0.1MnO2 composite as a cathode for sodium ion batteries. *RSC Adv.* **6**, 54404–54409 (2016).
32. Zhang, M., Hou, S., Li, Y., Hou, Y. & Yang, P. Single evaluation and selection of functional groups containing N or O atoms to heavy metal adsorption: Law of electric neutrality. *Chemosphere* **287**, 132207 (2022).
33. Yang, X. et al. Surface functional groups of carbon-based adsorbents and their roles in the removal of heavy metals from aqueous solutions: A critical review. *Chem. Eng. J.* **366**, 608–621 (2019).
34. Phoungthong, K. & Suwunwong, T. Magnetic biochar derived from sewage sludge of concentrated natural rubber latex (CNRL) for the removal of Al3 + and Cu2 + ions from wastewater. *Res. Chem. Intermed.* **46**, 385–407 (2020).
35. Jamil, S. et al. Synthesis of Saucer shaped manganese oxide nanoparticles by co-precipitation method and the application as fuel additive. *J. Clust Sci.* **29**, 1099–1106 (2018).
36. Zhang, J., Chen, M., Ge, Y. & Liu, Q. Manganese oxide on carbon fabric for flexible supercapacitors. *J. Nanomater.* **2016**, 2870761 (2016).
37. Chen, C., Liang, B., Ogino, A., Wang, X. & Nagatsu, M. Oxygen functionalisation of multiwall carbon nanotubes by microwave-excited surface-wave plasma treatment. *J. Phys. Chem. C.* **113**, 7659–7665 (2009).
38. Luo, C., Wei, R., Guo, D., Zhang, S. & Yan, S. Adsorption behavior of MnO2 functionalised multi-walled carbon nanotubes for the removal of cadmium from aqueous solutions. *Chem. Eng. J.* **225**, 406–415 (2013).
39. Hu, C., Liu, F., Lan, H., Liu, H. & Qu, J. Preparation of a manganese dioxide/carbon fiber electrode for electrosorptive removal of copper ions from water. *J. Colloid Interface Sci.* **446**, 359–365 (2015).

40. Suzuki, K., Kato, T., Fuchida, S. & Tokoro, C. Removal mechanisms of cadmium by δ-MnO2 in adsorption and co-precipitation processes at pH 6. *Chem. Geol.* **550**, 119744 (2020).
41. Kang, Y. L., Poon, M. Y., Monash, P., Ibrahim, S. & Saravanan, P. Surface chemistry and adsorption mechanism of cadmium ion on activated carbon derived from Garcinia mangostana shell. *Korean J. Chem. Eng.* **30**, 1904–1910 (2013).
42. Jung, H. J. Adsorption Characteristics of nickel, zinc and cadmium ions using alginate bead. *J. Chosun Nat. Sci.* **4**, 130–136 (2011).
43. Pirveysian, M. & Ghiaci, M. Synthesis and characterisation of sulfur functionalised graphene oxide nanosheets as efficient sorbent for removal of Pb2+, Cd2+, Ni2 + and Zn2 + ions from aqueous solution: a combined thermodynamic and kinetic studies. *Appl. Surf. Sci.* **428**, 98–109 (2018).
44. Alkurdi, S. S. A., Al-Juboori, R. A., Bundschuh, J., Bowtell, L. & Marchuk, A. Inorganic arsenic species removal from water using bone char: A detailed study on adsorption kinetic and isotherm models using error functions analysis. *J. Hazard. Mater.* **405**, 124112 (2021).
45. Wang, H. et al. Removal of pb(II), Cu(II), and cd(II) from aqueous solutions by biochar derived from KMnO4 treated hickory wood. *Bioresour Technol.* **197**, 356–362 (2015).
46. Asuquo, E., Martin, A., Nzerem, P., Siperstein, F. & Fan, X. Adsorption of cd(II) and pb(II) ions from aqueous solutions using mesoporous activated carbon adsorbent: equilibrium, kinetics and characterisation studies. *J. Environ. Chem. Eng.* **5**, 679–698 (2017).
47. Chen, C. et al. Preparation of MCS from low-grade bauxite desilication lye and adsorption of heavy metals. *Materials* **16**, 3506 (2023).
48. Tangarfa, M., Aouragh Hassani, S., Alaoui, A. & N. & Behavior and mechanism of tannic acid adsorption on the calcite surface: Isothermal, kinetic, and thermodynamic studies. *ACS Omega*. **4**, 19647–19654 (2019).
49. Araújo, C. S. T. et al. Elucidation of mechanism involved in adsorption of pb(II) onto lobeira fruit (Solanum lycocarpum) using langmuir, freundlich and temkin isotherms. *Microchem. J.* **137**, 348–354 (2018).
50. Kuczajowska-Zadrożna, M., Filipkowska, U. & Jóźwiak, T. Adsorption of Cu (II) and cd (II) from aqueous solutions by chitosan immobilised in alginate beads. *J. Environ. Chem. Eng.* **8**, 103878 (2020).
51. Guo, T. et al. Mechanism of cd(II) and Cu(II) Adsorption onto few-layered magnetic graphene oxide as an efficient adsorbent. *ACS Omega*. **25**, 16535–16545 (2021).
52. Pang, Y. et al. Cadmium adsorption performance and mechanism from aqueous solution using red mud modified with amorphous MnO_2. *Sci. Rep.* **12**, 4424 (2022).
53. Zhou, L. et al. Adsorption properties of Nano-MnO2–Biochar composites for copper in aqueous solution. *Molecules 2017*. **22**, 173 (2017).
54. Tumampos, S. B. et al. Isotherm, kinetics and thermodynamics of Cu(II) and Pb(II) adsorption on groundwater treatment sludge-derived manganese dioxide for wastewater treatment applications. *Int. J. Environ. Res. Publ. Health* **18**, 3050 (2021).
55. Meng, K. et al. Efficient adsorption of the cd(II) and as(V) using novel adsorbent ferrihydrite/manganese dioxide composites. *ACS Omega* **4**, 18627–18636 (2019).
56. Qammar, H., Gładyszewski, K., Górak, A. & Skiborowski, M. Towards the development of advanced packing design for distillation in rotating packed beds. *Chem. Ing. Tech.* **91**, 1663–1673 (2019).
57. Shim, J. W., Park, S. J. & Ryu, S. K. Effect of modification with HNO3 and NaOH on metal adsorption by pitch-based activated carbon fibers. *Carbon N Y.* **39**, 1635–1642 (2001).
58. Yu, J. et al. High adsorptivity and recycling performance activated carbon fibers for Cu(II) adsorption. *Sci. Total Environ.* **700**, 134412 (2020).
59. Nasruddin, M. N., Fahmi, M. R., Abidin, C. Z. A. & Yen, T. S. Regeneration of spent activated carbon from wastewater treatment plant application. *J. Phys. Conf. Ser.* **1116**, 032022 (2018).
60. Lingamdinne, L. P. et al. Magnetic-watermelon rinds biochar for uranium-contaminated water treatment using an electromagnetic semi-batch column with removal mechanistic investigations. *Chemosphere* **286**, 131776 (2022).
61. Angaru, G. K. R. et al. Portable SA/CMC entrapped bimetallic magnetic fly ash zeolite spheres for heavy metals contaminated industrial effluents treatment via batch and column studies. *Sci. Rep.* **12**, 1–17 (2022).
62. Fernandez, R. M. D. et al. Experimental design and breakthrough curve modeling of fixed-Bed columns utilising a novel 3D coconut-based polyurethane-activated carbon composite adsorbent for lead sequestration. *Sustain. 2023*. **15**, 14344 (2023).
63. Chen, C. et al. Dynamic adsorption models and artificial neural network prediction of mercury adsorption by a dendrimer-grafted polyacrylonitrile fiber in fixed-bed column. *J. Clean. Prod.* **310**, 127511 (2021).
64. Deng, X. et al. Adsorption performance and physicochemical mechanism of MnO2-polyethylenimine-tannic acid composites for the removal of Cu(II) and cr(VI) from aqueous solution. *Front. Chem. Sci. Eng.* **15**, 538–551 (2021).

Acknowledgements

This research was supported by the Basic Science Research Program through the National Research Foundation of Korea (NRF), funded by the Ministry of Education (2021R1A6A1A03038785) and as well as by his research was supported by the research fund of Seoul Green Environment Centre (23-01-03-04-25), Korea Environmental Industry and Technology Institute (RS-2023-00230606). This work was supported by a Kwangwoon University research grant in 2024 in Seoul, Korea.

Author contributions

Chandrika Ashwinikumar Pal, Yu-Lim Choi, Lakshmi Prasanna Lingamdinne: Conceptualization, Investigation, Writing, Original Draft; Rakesh Kulkarni: Data Analysis and Validation; Rama Rao Karri: Writing, Review-editing; Janardhan Reddy Koduru, Yoon-Young Chang: Methodology, Supervision, Validation and Funding Acquisition.

Declarations

Competing interests

The authors declare no competing interests.

Additional information

Supplementary Information The online version contains supplementary material available at https://doi.org/10.1038/s41598-024-84872-5.

Correspondence and requests for materials should be addressed to R.R.K., J.R.K. or Y.-Y.C.